Applied Catalysis B: Environmental 198 (2016) 142–153

Contents lists available at ScienceDirect

Applied Catalysis B: Environmental

journal homepage: www.elsevier.com/locate/apcatb

Stability of 3D-porous Ni/Cu cathodes under real alkaline electrolyzer operating conditions and its effect on catalytic activity

Carlos Valero-Vidal[a,b,*,1], Isaac Herraiz-Cardona[a,c,1], Valentín Pérez-Herranz[a], Anna Igual-Muñoz[a]

[a] Ingeniería Electroquímica y Corrosión (IEC), Departamento de Ingeniería Química y Nuclear, Universitat Politècnica de València, Camí de Vera s/n, 46022, Spain
[b] Advanced Light Source (ALS) and Joint Center for Energy Storage Research (JCESR), Lawrence Berkeley National Laboratory, 1 Cyclotron Rd., Berkeley, CA 94720, USA
[c] Institute of Advanced Materials (INAM), Universitat Jaume I, Castelló 12006, Spain

ARTICLE INFO

Article history:
Received 1 March 2016
Received in revised form 11 May 2016
Accepted 16 May 2016
Available online 20 May 2016

Keywords:
Hydrogen evolution reaction (HER)
Service life tests
Alkaline water electrolyzers
Ni/Cu cathodes

ABSTRACT

Despite the development and synthesis of new electrode materials for hydrogen generation in alkaline water electrolyzers has been a research topic widely exploited in the last years, stability tests on the obtained cathodes have been restricted to long-term potentiostatic/galvanostatic experiments which do not fulfil the real operating conditions that take place in those devices. In this work, two different Service Life Tests have been designed and implemented, aiming at including particular conditions (i.e. inverse polarity and short-circuit) in the durability and catalytic activity of cathode characterization. For this purpose, Ni/Cu bilayered porous electrodes were prepared using different Ni electrodeposition times (15, 30 and 45 min) following a double template electrochemical method. It has been confirmed that the electrode with the lowest Ni content can be considered as a promising electrocatalyst for hydrogen production under industrial conditions because of its optimal activity and stability after the two sets of testing conditions. In particular, electrochemical studies demonstrated that an inversion in polarity can positively affect the electrode performance, as a consequence of the synergetic interaction between $CuO/Cu(OH)_2$ and β-$Ni(OH)_2$ species formed at potentials below the oxygen evolution domain.

1. Introduction

Hydrogen is considered an ideal energy carrier that can be an alternative to fossil fuels because of its high energy density, versatility, good efficiency, full recyclability with a practical unlimited supplied and clean energy source [1–6]. Alkaline water electrolysis is one of the most promising methods of electrochemical hydrogen production since it allows obtaining significant hydrogen yields with high purity. Furthermore, this technique presents an environmental friendly technology since it can be coupled to other renewable energy systems [7]. Nevertheless, the considerably high operating costs of alkaline water electrolyzers, mainly due to the high overpotentials of the hydrogen/oxygen production and the lack of stability of the electrode materials, constitutes still an issue for large- scale applications.

In order to solve the energetic problems associated to alkaline electrolyzers, research efforts are focused on the development of new cathodes, which provide an enhancement in the catalytic activity for hydrogen evolution reaction (HER) together with an improved stability for long-term operation. Nickel has been one of the most widely employed low-cost alternative for Pt-group metals (such as Pt, Rh, Ir, and Pd) for HER, and similar catalytic activity has been reported by following different strategies [8–17]. The most extended alternatives to increase the activity of the Ni electrodes towards HER are *(i)* increasing its active surface area in order to have more active centers in a defined geometrical area (apparent activity), and *(ii)* finding a synergistic effect with other transitions elements with similar catalytic activity (such as Co, Cu, Fe and/or Mo among others) [18–24]. The latter produces a modification in the electronic distribution of the Ni which can lead to a decrease

* Corresponding author at: Ingeniería Electroquímica y Corrosión (IEC), Departamento de Ingeniería Química y Nuclear, Universitat Politècnica de València, Camí de Vera s/n, 46022, Spain.
E-mail addresses: cvalerovidal@lbl.gov, c.valerovidal@gmail.com (C. Valero-Vidal), iherraiz@uji.es (I. Herraiz-Cardona).
[1] These authors have contributed equally to the paper.

http://dx.doi.org/10.1016/j.apcatb.2016.05.030
0926-3373/

in activation energy for HER, thus improving their intrinsic activity [25].

Synergistic interaction of Ni and Cu towards the improvement of the catalytic activity for HER has been studied by different authors [26,27]. Solmaz et al. [26] found that the HER activity for NiCu porous composites, galvanostatically electrodeposited on Cu, was higher than that obtained for uncoated and Ni coated electrodes. They attributed this behavior to the electrode porosity as well as the synergetic interaction between both elements. In addition, these authors confirmed that NiCu composites presented a good time stability and corrosion resistance for electrolysis [28]. In a recent published work, Ngamlerdpokin and Tantavichet [27] demonstrated that electrocatalytic activity for HER depends on the composition of NiCu alloys, and high electrocatalytic activity was achieved for electrodes with higher Cu/Ni composition ratio.

Stability testing of the selected cathodes is a mandatory step that must be taken into account due to the aggressive operation conditions of those electrolyzers (i.e. concentrated alkaline solution of KOH between 25 and 30% at temperature ranging from 80 °C to 90 °C) [29–32] . Furthermore, an important phenomenon of *inverse polarization* take place in industrial electrolyzers when the process is interrupted for different situations: maintenance, electrolyte and electrodes replacement as a consequence of the loss of their activity, installation of new cells, accidental trips of safety systems and/or unplanned interruptions of the power supply among others. During those processes, anodes and cathodes are *short-circuited*, and due to the change in the equilibrium conditions with respect to the vigorous hydrogen discharge, cathodes become anodically polarized while anodes become cathodically polarized, causing a reverse current flow between the electrodes. The *short-circuited* situation and the reverse current flow can generate modifications in the cathode composition, which could negatively affect their activity for further hydrogen discharges [33,34]. Different strategies have been carried out by several authors in order to monitor and analyze the electrochemical behavior of the electrodes under long term and short-circuited situations and, therefore, to predict how this operation can affect their performance [35–38] .

The purpose of this work is to analyze the electrocatalytic activity and stability for HER of 3D-porous cathodes synthetized by a two-step electrodeposition method of Ni onto Cu foams. The electrocatalytic performance of the developed electrodes was analyzed by electrochemical techniques and their stability was evaluated using two different *Service Life Tests*, which properly simulate the whole range of possible conditions in typical and particular alkaline water electrolysis in 30 wt.% KOH solution at 80 °C. The main impact of this paper is to understand the role of the underlying Cu foam in the catalytic activity and stability towards HER in the synthetized Ni/Cu-cathodes when those are reversely polarized.

2. Experimental

2.1. Synthesis of the electrodes

Porous coatings were deposited on AISI 304 stainless steel substrates embedded in Teflon with a cross-section available area of 0.5 cm^2. As a previous step, stainless steel substrates were pretreated by the usual procedure described elsewhere [39–42] .

Initially, a 3D-porous Cu structure was obtained by electrodeposition following our previous work [42]. In brief, an acidic bath with a chemical composition of 0.05 M $CuSO_4$ and 0.5 M H_2SO_4 was used at room temperature, and a constant current density of −0.2 A cm^{-2} during 450 s was applied. During the galvanostatic Cu electrodeposition, the generated H_2 bubbles acted as a dynamic template to build up 3D foam Cu structure, as schematically described in Ref. [42].

Table 1
Operating conditions employed in the synthesis of Ni/Cu porous electrodes.

	Cu template formation		Ni electrodeposition	
	Bath composition/M		Bath composition/M	
Catalyst	$CuSO_4$	0.05	$NiSO_4$	1.26
	H_2SO_4	0.5	$NiCl_2$	0.19
			H_3BO_4	0.60
	i/A cm^{-2}	Time/s	i/A cm^{-2}	Time/s
ED1	0.2	450	0.05	900
ED2	0.2	450	0.05	1800
ED3	0.2	450	0.05	2700

Ni was electrodeposited onto the initial formed Cu macroporous coating from a modified Watts bath (1.26 M $NiSO_4$, 0.19 M $NiCl_2$, 0.6 M H_3BO_3) under galvanostatic conditions of −0.025 A cm^{-2} and 50 °C. Thus, the underlying Cu structure served as a template for the subsequent Ni deposit. Ni electrodeposition times of 15 (ED1), 30 (ED2) and 45 min (ED3) were employed.

The bath compositions and the electrodeposition conditions for the different synthetized porous electrodes (named ED1, ED2 and ED3) are summarized in Table 1.

A double walled and vertical three-electrode cell (with an electrolyte volume of 50 mL) was used to obtain Cu- and Ni-electrodeposits as represented in Ref. [20]. The surface of the substrate was placed horizontally at the bottom part of the cell, thus allowing the free release of H_2 bubbles. A commercial Ag/AgCl (3 M KCl) was used as a reference electrode and a Pt electrode as a counter electrode. Electrochemical measurements were controlled using an AUTOLAB PGSTAT302 N potentiostat/galvanostat.

The structure, morphology and chemical composition of the electrocatalytic coatings were evaluated using a JEOL JSM-3600 Scanning Electron Microscope (SEM) coupled with an Energy Dispersed X-Ray (EDX).

2.2. Electrochemical measurements

Two different electrochemical tests were conducted in order to characterize both the catalytic activity for HER and stability (*Service Life Tests*) of the synthetized Ni/Cu cathodes:

(a) A galvanostatic measurement (1 h at −0.1 A cm^{-2}) was initially performed with the aim to activate the electrodes and for establishing reproducible conditions. Polarization curves (recorded from −1.6 V up to the equilibrium potential at the scan rate of 1 mV s^{-1}) and electrochemical impedance spectroscopy (EIS) measurements were carried out for characterizing the catalytic activity towards HER of the as-prepared electrodes. EIS was carried out at different cathodic overpotentials (HER region), and performed for 10 frequency per decade from 10 kHz to 3 mHz with an amplitude of ± 10 mV. Obtained spectra were analyzed using Zview 2.70 software package and fitted with the corresponding electrical equivalent circuit (EEC).

First Service Life Test (*1SLT*) was proposed in order to study the effect of anodic potential on the catalytic activity of the synthetized cathodes. Potentiostatic tests at potential below (0.25 V) and above (0.75 V) oxygen evolution reaction (OER) during 30 min were applied. Onset of OER yields around 0.35 V in the synthetized cathodes. After each potentiostatic test, polarization curve and EIS measurements were performed under the same conditions above described. Fig. 1(a) shows schematically the experimental sequence of the *1SLT*.

(b) The *Second Service Life* test (*2SLT*) consisted basically of three stages where the last two were repeated 10 times: galvanos-

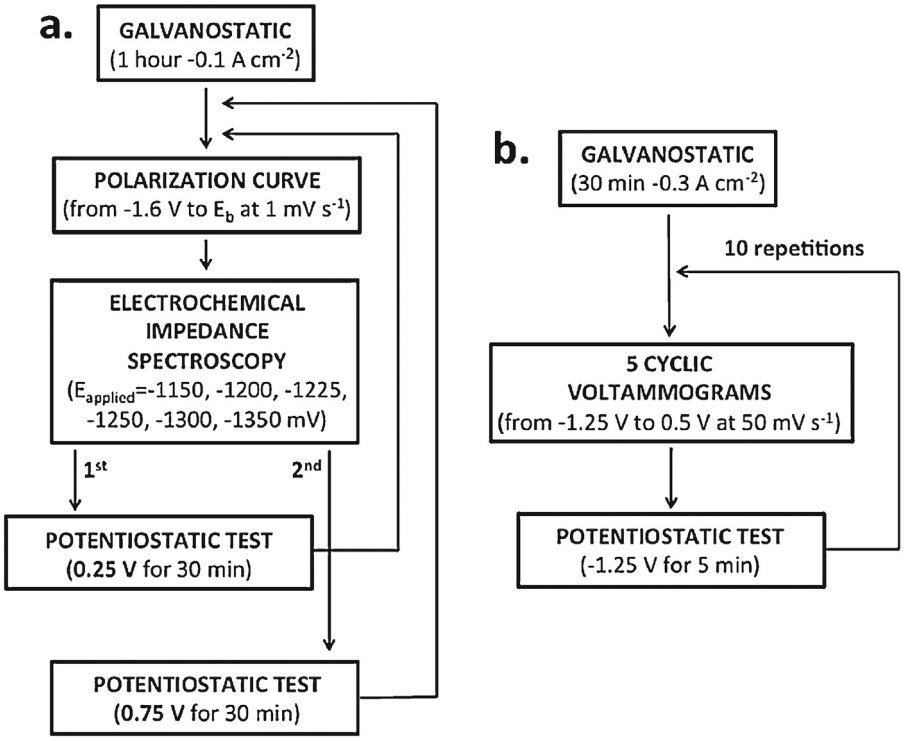

Fig. 1. Electrochemical techniques sequence of the proposed *Service Life Tests* in order to study the stability of the cathodes towards the HER: (a) *SLT1* aims to study the effect of the anodic potential in the stability for HER (b) *SLT2* simulates process of polarization inversion carried out in the electrolysers when the electrodes are replaced.

tatic measurements (at -0.3 A cm^{-2} during 30 min), series of 5 CV from -1.25 to 0.5 V (potential range between HER and OER) at a scan rate of 50 mV s^{-1} and potentiostatic test at the applied potential of -1.25 V during 300 s (H_2 discharge). A simulation of the short-circuited and inverse polarization conditions, occurred in the industrial electrolyzers when electrodes are replaced after intervals of H_2 discharge, was carried out using *2SLT*, represented in Fig. 1(b). In addition, first series of 5 CVs (before H_2 discharge) for each were used for the initial electrochemical characterization of the as-prepared cathodes.

With the aim of comparing the results, both tests were also systematically performed on commercial Ni and Cu substrates, previously abraded with emery paper down to 4000 grit, and polished with alumina paste (1 μm) to get a mirror-like surface finishing (*smooth Ni* and *smooth Cu*, respectively). All experimental tests were carried out in an oxygen free atmosphere, 30 wt.% KOH solution at 80 °C, which corresponds to the industrial conditions in alkaline electrolysis. Three repetitions of *(a)* and *(b)* in all the studied cathodes were performed to verify the reproducibility of the electrochemical measurements.

The electrochemical measurements were carried out in a specific design of an electrochemical cell [43]. The synthetized electrodes were used as a working electrodes placed on a vertical plane to allow for the elimination of the produced hydrogen bubbles. The counter electrode was a large-area Ni foam (INCOFOAM^{TM}) and the reference electrode was the Ag/AgCl electrode. All potentials are given with respect to the Ag/AgCl electrode which has a standard potential of 197 mV with respect to the standard hydrogen electrode (SHE). The experiments were done by using an AUTOLAB PGSTAT302 N potentiostat/galvanostat. A schema of the experimental setup and the electrochemical cell used in this work was shown in a previous published work [20].

3. Results and discussion

3.1. Initial characterization of as-prepared cathodes

Surface morphology of the synthetized cathodes at the three different electrodeposition times of Ni can be observed through the SEM images shown in Fig. 2. All the deposits present a porous structure with a more rounded shape as the Ni electrodeposition time increases. Thus, the microstructure of the coating changes from the finger-like (Fig. 2(a)) to the cauliflower-like structure (Fig. 2(c)). Nickel fills the gaps of the foam walls and makes much denser the ramified structure (mechanism described in detail in Ref. [42]). Additionally, a size enlargement of the nickel nucleus initially formed (observed in ED1) is detected in ED3.

The atomic percentage of Cu detected by EDX in the deposits decreases with the Ni deposition time from 33.41 at.% at 15 min (ED1) to 9.81 at.% at 30 min (ED2), and completely disappears after 45 min of Ni deposition (ED3), Table 2. On ED1 and ED2, it was detected by local EDX analysis that Ni-richest regions are placed in the outer parts of the pores, whereas inside the pores the Ni content considerably decreases, as a consequence of a heterogeneous current distribution during the electrodeposition. This indicates that either Ni electrodeposition time below 45 min does not completely cover the underlying Cu foam template or the Ni layer thickness is lower than the X-ray penetration length. To qualitatively conclude on the real composition of the electrode surface in contact

Table 2
Superficial composition of the developed electrodes determined by EDX.

Electrode	Deposition time (min)	at.%	
		Ni	Cu
ED1	15	66.59	33.41
ED2	30	90.19	9.81
ED3	45	100	0

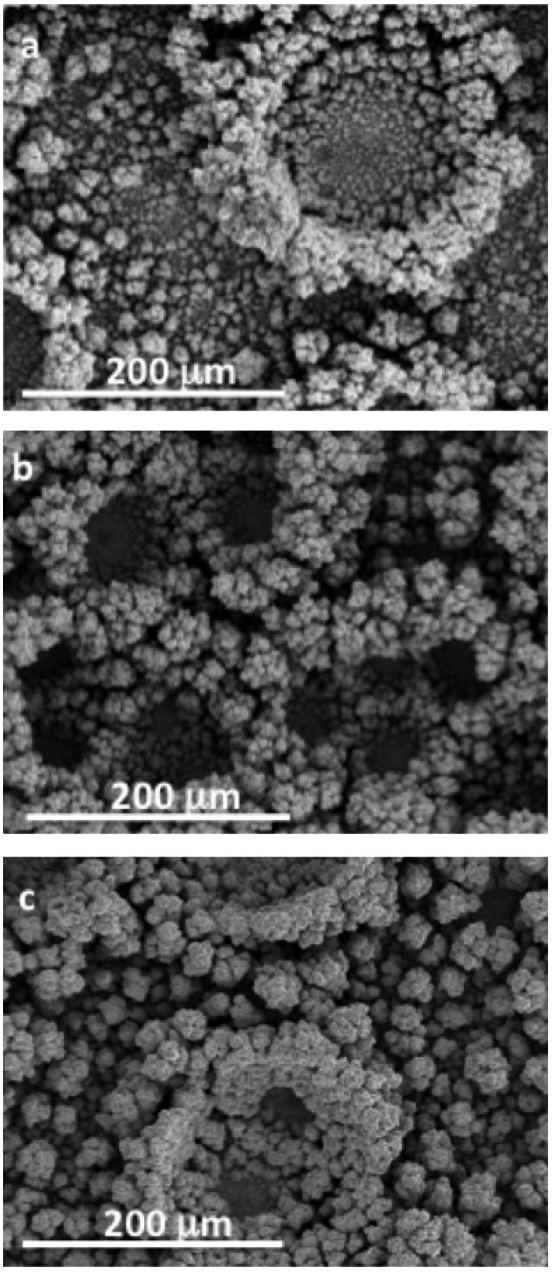

Fig. 2. SEM images of the porous cathodes after (a) 15 min (ED1), (b) 30 min (ED2) and (c) 45 min (ED3) Ni electrodeposition times on the Cu template.

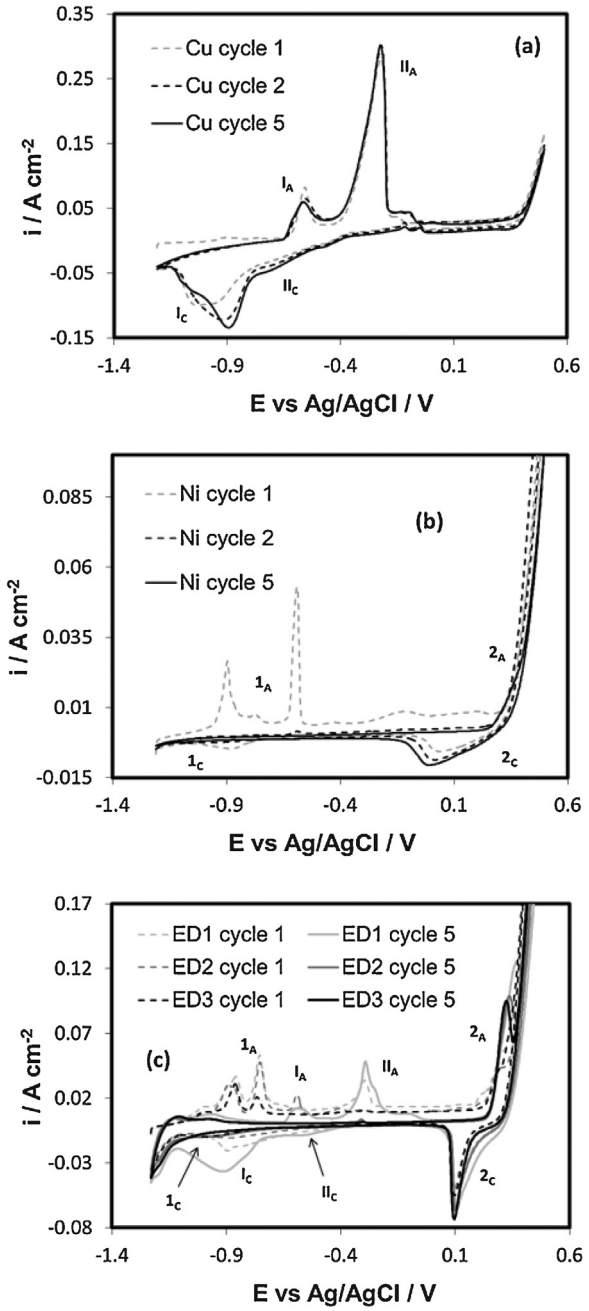

Fig. 3. First 5 cyclic voltammograms obtained for (a) Cu (b) Ni and (c) ED1-ED2-ED3 porous cathodes between the potential region from hydrogen evolution (-1.25 V) to oxygen evolution (0.5 V) in KOH 30 wt.% at 80 °C and at the sweep rate of 50 mV s^{-1}.

with the electrolyte, an initial cyclic voltammetry study has been performed on commercial smooth Cu and Ni electrodes, and on the electrodeposits, as depicted in Fig. 3.

The cyclic voltammetry of smooth Cu (Fig. 3(a)) shows two oxidation peaks, I_A (−581 mV) and II_A (−238 mV), corresponding to the formation of Cu(I) and Cu(II) oxides, respectively. The anodic peak I_A corresponds to the oxidation of Cu to CuOH which is insoluble at this pH and subsequently is transformed to Cu_2O (Eq. (1)) [44,45] . The broad anodic peak II_A corresponds to the formation of a thick multilayered film of CuO and Cu $(OH)_2$ (Eqs. (2) and (3)) [45–48]. The ratio between the peaks I_A and II_A shows that CuO is mainly formed from Cu via the two-electron oxidation reaction (Eq. (4)) although CuO can also be obtained by the oxidation of Cu_2O in a less extent.

$$2Cu + 2OH^- \rightarrow Cu_2O \cdot H_2O + 2e^- \quad (1)$$

$$Cu_2O + 2OH^- + H_2O \rightarrow 2Cu(OH)_2 + 2e^- \quad (2)$$

$$Cu_2O + 2OH^- \rightarrow 2CuO + H_2O + 2e^- \quad (3)$$

$$2Cu + 2OH^- \rightarrow 2CuO + H_2 + 2e^- \quad (4)$$

On the reverse cathodic scan, the reduction peak II_C (−664 mV) is associated with the reduction of Cu(II) to Cu(I) and the peak I_C (−975 mV) with the reduction of Cu(I) to Cu. Thus, under the studied conditions, the peak II_C corresponds to the reduction of $Cu(OH)_2$ to Cu_2O (Eq. (5)), whereas the peak I_C is attributed to the reduction of Cu(I) hydrous oxide to a Cu adatom [49] and to the reduction of Cu_2O to the metal (Eq. (6)).

$$2Cu(OH)_2 + 2e^- \rightarrow Cu_2O + 2OH^- + H_2O \quad (5)$$

$$Cu_2O + H_2O + 2e^- \rightarrow 2Cu + 2OH^- \quad (6)$$

Cyclic voltamograms of smooth Ni are shown in Fig. 3(b). The anodic peaks 1_A (−900 mV and −596 mV) and 2_A (141 mV) are related to the oxidation of Ni to Ni(II) and Ni(II) to Ni(III), respectively. The peaks 1_A are related to the formation of $Ni(OH)_2$ (Eq. (7)), in particular to the irreversible formation of a reducible phase (α-$Ni(OH)_2$) into a non-reducible phase (β-$Ni(OH)_2$), respectively [50]. The reduction of the passive layer composed by Ni(II) is potential dependent, and its reduction is not possible when the anodic potential is above −0.7 V [51,52]. The presence of this non-reducible phase in the oxide layer is confirmed by the absence of the anodic peak 1_A during the second anodic scan. The peak 2_A corresponds to the oxidation of β-$Ni(OH)_2$ into β-NiOOH (Eq. (8)), which appears overlapped with the increase of the current density because of OER.

$$Ni + 2OH^- \rightarrow Ni(OH)_2 + 2e^- \quad (7)$$

$$\beta - Ni(OH)_2 + OH^- \rightarrow \beta - NiOOH + H_2O + e^- \quad (8)$$

In the negative-going scan, the peak 2_C (64 mV) shows the reduction of Ni(III) to Ni(II) and the peak 1_C (−880 mV) the reduction of Ni(II) to Ni. In this, the peak 2_C corresponds to the reduction of NiOOH to β-$Ni(OH)_2$ which is typical for the Ni- based cathodes (Eq. (9)) [35,53]. On the other hand, the peak 1_C presents the reduction of the reducible phase α-$Ni(OH)_2$ into Ni. This is relatively small due to the small amount of residual α-$Ni(OH)_2$ presented in the electrode which was not converted into β-$Ni(OH)_2$ during the first scan. In the second scan, the disappearance of the peak 1_C confirms the fact that all Ni is converted into β-$Ni(OH)_2$.

$$\beta - NiOOH + H_2O + e^- \rightarrow \beta - Ni(OH)_2 + OH^- \quad (9)$$

Cyclic voltammograms obtained on ED1, ED2 and ED3 coatings are represented in Fig. 3(c). Only cycles 1 and 5 were plotted to clearly distinguish the characteristic current peaks. In the electrodes ED1 and ED2, the contribution of the peaks I_A and II_A are detected and are associated to the formation of Cu_2O and $CuO/Cu(OH)_2$ oxides respectively, as already described. Stronger contribution of these peaks was observed in the coating ED1 due to the higher amount of Cu in contact with the electrolyte from the macroporous structure. These results confirm that Ni electrodeposition time up to 30 min is not sufficient to completely cover the underlying Cu template. This phenomenon was attributed to a heterogeneous current distribution during the electrodeposition of Ni, being the outer parts of the pores preferentially covered, which was confirmed by local EDX analysis. Therefore, the Ni-free copper regions of the electrode surface actively participate in the electrochemical behavior of the electrodes.

On the other hand, peaks 1_A, 2_A and 2_C are observed in the CVs of the three electrodes and correspond to the electrochemical behavior detected for the smooth Ni electrode (Fig. 3(b)). However, a considerable increase of charge in the redox system 2_A–2_C and a well-defined onset of the HER (−1.25 V) evidenced the increase of the active surface area in the synthetized electrodes.

3.2. Activity for HER of the synthetized cathodes

Fig. 4 shows the Tafel curves obtained on the investigated electrodes, and on Ni and Cu smooth bulk electrodes in 30 wt.% KOH at 80 °C. The curves were corrected to the reversible HER potential at the given conditions and for the ohmic drop ($j \cdot R_S$), estimating the solution resistance, R_S, from the EIS measurements.

A linear behavior was observed in all polarization curves (Fig. 4) which denotes that HER on these electrodes is kinetically controlled, i.e. described by the Tafel equation (see *Supporting information*, SI) [42,54]. Values of the Tafel slope (b, mV dec^{-1}), the exchange current density (j_0, mA cm^{-2}) and the charge transfer coefficient (α) obtained after fitting by a linear regression the polarization curves are summarized in Table 3. When two different slopes were observed (i.e. in the case of Cu), the slope obtained in the range of higher current densities (higher than −0.3 A cm^{-2}) was considered since this current range is characteristic of the cathodes working under industrial conditions. All the synthetized electrodes show higher activity towards HER than the pure Ni, which can be initially attributed to the enhancement of the active surface area. Moreover, according to the extracted parameters, b in the range of 115–130 mV dec^{-1} and α close to 0.5–0.6 for all the coatings, HER proceeds via Volmer (Eq. (10))-Heyrovsky (Eq. (11)) mechanism [10,55–60]. This mechanism of HER involves the formation of an adsorbed hydrogen atom intermediate MH_{ads} (Volmer reaction) followed by an electrochemical hydrogen desorption step (Heyrovsky reaction).

$$H_2O + M + e^- \rightarrow MH_{ads} + OH^- \quad (10)$$

$$H_2O + MH_{ads} + e^- \rightarrow H_2 + M + OH^- \quad (11)$$

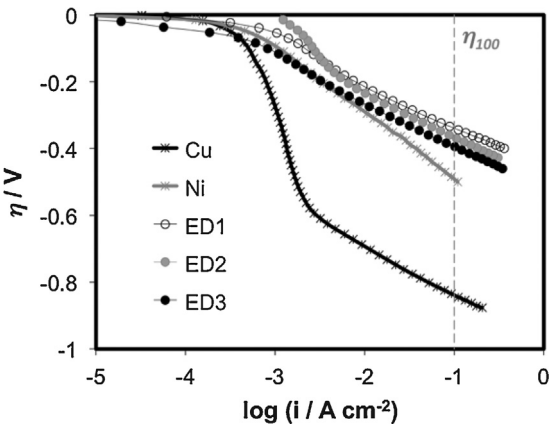

Fig. 4. Linear Tafel polarization curves recorded on Cu, Ni and the different developed cathodes (ED1, ED2 and ED3) in 30 wt.% KOH solution at 80 °C (scan rate 1 mV s^{-1}).

Table 3
HER kinetic parameters extracted from the polarization curves obtained in the Cu, Ni and catalytic electrodes in 30 wt.% KOH solution at 80 °C.

Electrode	As-prepared	0.25 V	0.75 V
Cu			
b/mV dec^{-1}	144.5	185.5	252.4
α	0.48	0.38	0.28
j_0/μA cm^{-2}	0.2	2.4	12.5
$\lvert\eta_{100}\rvert$ (mV)	839	850	950
Ni			
b/mV dec^{-1}	119.1	206.2	199.7
α	0.37	0.34	0.35
j_0/mA cm^{-2}	0.30	0.82	0.13
$\lvert\eta_{100}\rvert$ (mV)	490	439	579
ED1			
b/mV dec^{-1}	117.4	99.3	95.7
α	0.60	0.71	0.73
j_0/mA cm^{-2}	0.14	1.03	0.22
$\lvert\eta_{100}\rvert$ (mV)	338	200	260
ED2			
b/mV dec^{-1}	129.9	97.1	88.9
α	0.54	0.72	0.79
j_0/mA cm^{-2}	0.15	0.51	0.44
$\lvert\eta_{100}\rvert$ (mV)	366	224	210
ED3			
b/mV dec^{-1}	128.5	94.1	95.1
α	0.55	0.74	0.74
j_0/mA cm^{-2}	0.09	0.40	0.48
$\lvert\eta_{100}\rvert$ (mV)	394	227	222

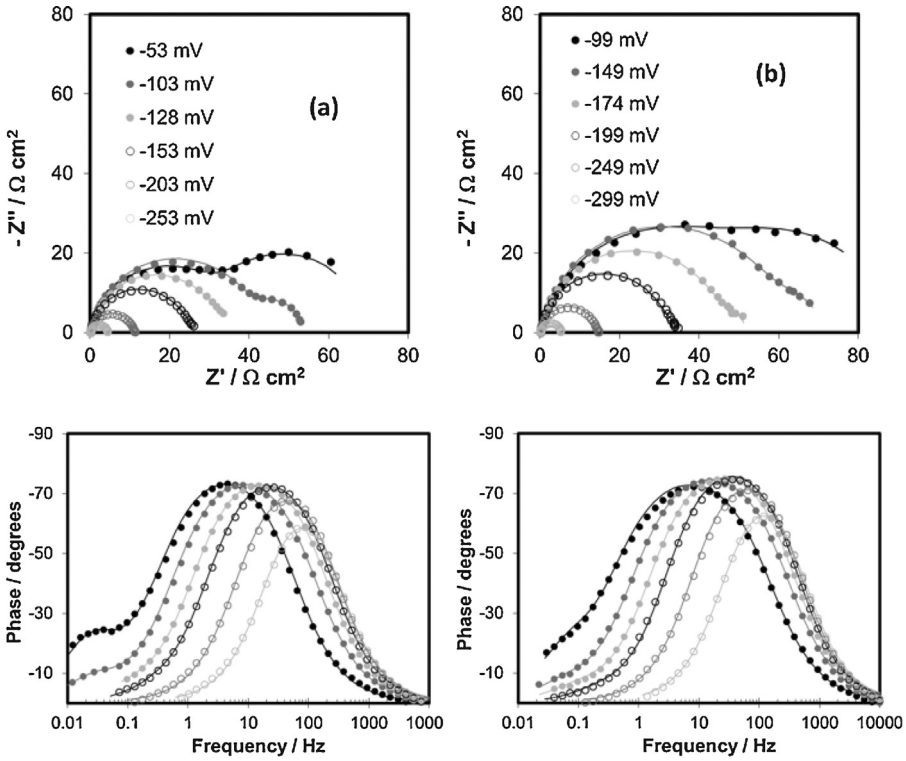

Fig. 5. Impedance data represented by Nyquist diagrams (up) and Bode plots (down) obtained in 30 wt.% KOH solution at 80 °C for (a) ED1 and (b) ED3 cathodes at different overpotentials. Experimental points are represented by symbols and modelled data by solid lines.

where M is a free site on the metal surface and MH_{ads} is the metal surface occupied by hydrogen adatoms.

Overpotential values of the cathodes at the fixed current of 100 mA cm^{-2} (η_{100}) were also extracted from the polarization curves in order to evaluate their apparent activity towards HER (included in Table 3). ED1 shows the lowest value of η_{100}, which indicates a reduction in the energy requirements to produce a fixed amount of hydrogen in comparison with the others cathodes.

A deeper insight into the electrochemical behavior of the electrodes was performed by electrochemical impedance spectroscopy (EIS). This technique allows us to determine the HER kinetics and also to quantify the real electrochemically active surface area of the porous structures. Fig. 5 shows Nyquist diagrams (up) and Bode plots (down) of (a) ED1 and (b) ED3 at different overpotentials. EIS response is characterized by two semicircles (i.e. two-time constants) which diameter considerably decreases with the applied cathodic overpotential. This behavior indicates that both time constants are connected with the electrode kinetics [13,61]. Equivalent electrical circuit (EEC) consisting of two-time constant in parallel (2TP) (Fig. 6(a)) was used to model the experimental EIS data. This model reflects the response of a HER system where the high frequency (*HF*) time constant is related to the charge transfer kinetics and the low frequency (*LF*) time constant is associated to the hydrogen adsorption [41,61–64].

The *LF* time constant in the spectra shown in Fig. 5 disappears at overpotentials below −200 mV. This effect indicates that the adsorption process is favored when high hydrogen discharge takes place and, thus, the charge-transfer process mainly dominates the impedance response when the cathodic potential increases. Here, HER is controlled by the Heyrovsky step [65–67]. In this case, a Randless circuit (Fig. 6(b)) which contains only one-time constant (1T) is used to describe the impedance response [68]. For both EEC, a constant phase angle element (CPE) is introduced to replace the double layer capacitance (C_{dl}) in order to take into account the non-ideal capacitive behavior [58,69]. CPE is defined in impedance representation as:

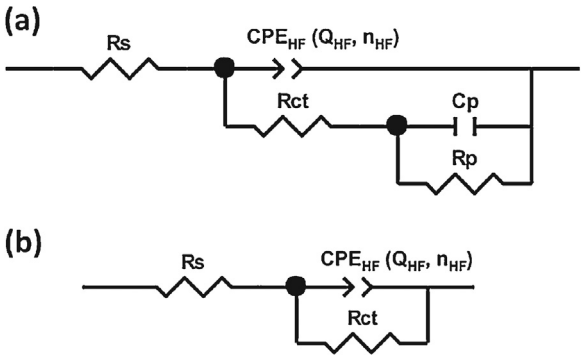

Fig. 6. EEC models used to explain the EIS response of the HER on the developed electrodes: (a) two-time constant parallel model (2TP) and (b) one-time constant (1T). In these, R_s is the solution resistance, CPE_{HF} is the high frequency constant phase element (composed by Q_{HF} and n_{HF}), R_{ct} is the charge transfer resistance, and C_p-R_p is the pseudocapacitance and the resistance related to the hydrogen adsorption, respectively.

$$Z_{CPE} = \left[Z_0 \times (i\omega)^n\right]^{-1} \quad (12)$$

where Z_0 is the CPE constant, ω is the angular frequency (in rad s^{-1}), $i^2 = -1$ is the imaginary number, and n is the CPE exponent.

The theoretical values of the electrical parameters obtained after fitting the experimental EIS spectra with 2TP/1 T EEC are compiled in Table 4. Lower Chi-squared values (X^2) and good fit estimation (plotted with continuous lines over the experimental data in Fig. 5) validate the selected EEC. The double layer capacitance related to

Table 4
EEC parameters obtained by fitting EIS experimental spectra recorded in the as-prepared electrocatalytic cathodes and after applying potentiostatic tests of 0.25 V and 0.75 V at various cathodic overpotentials in 30 wt.% KOH solution at 80 °C.

	Potential																	
	As-prepared						After 0.25 V						After 0.75 V					
ED_1 (15 min)																		
η/mV	−53	−103	−128	−153	−203	−253	−34	−84	−109	−134	−284	−234	−102	−152	−177	−202	−252	−302
X^2	4×10^{-4}	3×10^{-4}	4×10^{-4}	4×10^{-4}	2×10^{-4}	2×10^{-4}	6×10^{-4}	8×10^{-4}	8×10^{-4}	9×10^{-4}	5×10^{-4}	2×10^{-4}	5×10^{-4}	5×10^{-4}	5×10^{-4}	3×10^{-4}	3×10^{-4}	1×10^{-4}
$R_S/\Omega\,cm^2$	0.28	0.28	0.28	0.28	0.28	0.29	0.28	0.28	0.28	0.29	0.29	0.30	0.28	0.29	0.30	0.30	0.30	0.31
$R_{ct}/\Omega\,cm^2$	37.4	42.5	32.5	24.1	10.6	4.0	7.4	5.5	4.5	3.3	1.6	0.7	17.5	10.1	8.0	6.1	3.0	1.4
$R_P/\Omega\,cm^2$	31.2	10.7	3.0	1.5	–	–	19.3	2.2	0.7	0.2	–	–	31.7	5.1	2.1	0.8	–	–
$Q_{HF}/m\Omega^{-1}\,cm^{-2}\,s^n$	15.32	7.72	4.86	3.70	2.83	2.39	10.48	6.09	5.00	4.41	3.83	3.59	8.08	6.38	5.41	5.02	4.78	4.28
n_{HF}	0.92	0.91	0.92	0.94	0.95	0.97	0.91	0.94	0.94	0.95	0.96	0.97	0.87	0.90	0.92	0.92	0.93	0.95
$C_{dl}/mF\,cm^{-2^*}$	13.70	6.83	4.39	3.40	2.65	2.29	9.15	5.56	4.60	4.10	3.63	3.44	6.71	5.54	4.81	4.52	4.36	3.98
$C_P/F\,cm^{-2}$	0.28	0.64	0.51	0.36	–	–	0.22	0.99	1.78	4.36	–	–	0.14	0.45	0.78	1.35	–	–
τ_{HF}/s	0.51	0.29	0.14	0.08	0.03	0.01	0.07	0.03	0.02	0.01	5×10^{-3}	2×10^{-3}	0.12	0.06	0.04	0.03	0.01	6×10^{-3}
τ_{LF}/s	8.68	6.90	1.53	0.55	–	–	4.25	2.18	1.25	0.87	–	–	4.44	2.30	1.64	1.08	–	–
ED_2 (30 min)																		
η/mV	−61	−111	−136	−161	−211	−261	−51	−101	−126	−151	−201	−251	−64	−114	−139	−164	−214	−264
X^2	4×10^{-4}	4×10^{-4}	2×10^{-4}	2×10^{-4}	1×10^{-4}	1×10^{-4}	6×10^{-4}	9×10^{-4}	7×10^{-4}	7×10^{-4}	5×10^{-4}	3×10^{-4}	4×10^{-4}	4×10^{-4}	3×10^{-4}	2×10^{-4}	1×10^{-4}	1×10^{-4}
$R_S/\Omega\,cm^2$	0.27	0.27	0.27	0.27	0.27	0.27	0.27	0.27	0.27	0.27	0.27	0.28	0.27	0.28	0.31	0.33	0.35	0.38
$R_{ct}/\Omega\,cm^2$	49.7	58.4	44.3	32.8	15.8	5.5	20.1	14.1	10.9	8.0	4.2	1.7	38.9	23.7	23.2	20.2	8.6	3.4
$R_P/\Omega\,cm^2$	20.0	11.8	9.8	6.6	–	–	12.5	2.3	1.1	0.9	–	–	19.6	4.5	2.4	1.2	–	–
$Q_{HF}/m\Omega^{-1}\,cm^{-2}\,s^n$	6.21	3.32	2.35	1.97	1.79	1.56	3.33	2.73	2.36	2.05	2.03	1.72	2.86	2.69	2.40	2.29	2.27	2.16
n_{HF}	0.89	0.93	0.95	0.96	0.96	0.97	0.93	0.94	0.94	0.96	0.96	0.98	0.92	0.94	0.95	0.96	0.96	0.97
$C_{dl}/mF\,cm^{-2^*}$	5.28	3.01	2.19	1.86	1.69	1.50	3.01	2.49	2.18	1.93	1.90	1.67	2.53	2.47	2.25	2.17	2.18	2.09
$C_P/F\,cm^{-2}$	0.11	0.06	0.03	0.04	–	–	0.12	0.20	0.15	0.02	–	–	0.06	0.13	0.12	0.08	–	–
τ_{HF}/s	0.26	0.18	0.10	0.06	0.03	0.01	0.06	0.04	0.02	0.02	8×10^{-3}	3×10^{-3}	0.10	0.06	0.05	0.04	0.02	7×10^{-3}
τ_{LF}/s	2.20	0.71	0.29	0.26	–	–	1.50	0.46	0.17	0.02	–	–	1.18	0.59	0.29	0.10	–	–
ED_3 (45 min)																		
η/mV	−99	−149	−174	−199	−249	−299	−51	−101	−126	−152	−201	−251	−56	−106	−131	−156	−206	−256
X^2	4×10^{-4}	2×10^{-4}	2×10^{-4}	3×10^{-4}	2×10^{-4}	1×10^{-4}	7×10^{-4}	7×10^{-4}	5×10^{-4}	3×10^{-4}	1×10^{-4}	1×10^{-4}	4×10^{-4}	4×10^{-4}	4×10^{-4}	3×10^{-4}	1×10^{-4}	1×10^{-4}
$R_S/\Omega\,cm^2$	0.26	0.26	0.26	0.26	0.26	0.26	0.25	0.26	0.26	0.26	0.27	0.27	0.26	0.26	0.26	0.29	0.31	0.34
$R_{ct}/\Omega\,cm^2$	61.2	61.4	46.0	31.8	14.0	5.0	10.3	6.5	5.2	3.7	1.8	0.8	24.6	11.9	9.2	8.8	4.9	2.2
$R_P/\Omega\,cm^2$	26.2	9.2	5.5	2.4	–	–	13.5	1.5	0.6	0.2	–	–	29.8	4.2	1.7	0.9	–	–
$Q_{HF}/m\Omega^{-1}\,cm^{-2}\,s^n$	8.48	3.96	2.70	2.02	1.73	1.44	5.14	3.24	2.84	2.39	2.24	2.04	4.41	3.43	3.07	2.89	2.80	2.55
n_{HF}	0.89	0.91	0.93	0.95	0.96	0.97	0.92	0.94	0.94	0.96	0.96	0.98	0.89	0.92	0.92	0.93	0.94	0.95
$C_{dl}/mF\,cm^{-2^*}$	7.15	3.47	2.44	1.89	1.63	1.39	4.55	2.97	2.61	2.25	2.12	1.96	3.74	3.03	2.74	2.62	2.58	2.40
$C_P/F\,cm^{-2}$	0.11	0.34	0.35	0.35	–	–	0.37	1.00	2.12	0.10	–	–	0.17	0.48	0.55	0.92	–	–
τ_{HF}/s	0.44	0.21	0.11	0.06	0.02	0.01	0.05	0.02	0.01	0.01	4×10^{-3}	2×10^{-3}	0.09	0.04	0.03	0.02	0.01	5×10^{-3}
τ_{LF}/s	2.88	3.13	1.92	0.84	–	–	5.00	1.50	1.27	0.02	–	–	5.07	2.02	0.94	0.83	–	–

Table 5
Exchange current densities (j_o) corrected with the surface roughness factor (f_r) obtained from polarization curves in the as-prepared porous cathodes and after applying the potentiostatic tests of 0.25 V and 0.75 V in 30 wt.% KOH solution and 80 °C.

Electrode	$j_o \times f_r^{-1}$/μA cm^{-2}		
	As-prepared	0.25 V	0.75 V
ED1	0.20	2.26	0.66
ED2	0.58	3.41	3.48
ED3	0.24	1.74	2.54

the charge- transfer kinetics (C_{dl}) for the catalytic coatings were determined using the relation suggested by Brug et al. [70,71]:

$$C_{dl} = \left[\frac{Q_{HF}}{\left(R_S{}^{-1} + R_{ct}{}^{-1}\right)^{(1-n_{HF})}}\right]^{1/n_{HF}} \quad (13)$$

where Q_{HF} and n_{HF} are the components of the CPE_{HF}, R_s is the solution resistance, and R_{ct} is the charge transfer resistance. As expected, R_{ct} decreases with the cathodic overpotential suggesting an activation of the electrodes towards HER. The same trend is observed for the resistance associated to the hydrogen adsorption (R_p), which corresponds well to the response of hydrogen adsorbed on catalyst surfaces.

Real active surface area, in terms of surface roughness factor (f_r), was determined relating the C_{dl} of the porous and the smooth Ni electrode. A value of 20 μF cm^{-2} was used for the double layer capacitance of the smooth metallic surface, which was extracted from the literature [72–74] and also from previous works [39]. A decrease in f_r with the cathodic overpotential is observed for all electrodes (values shown in Table S1, SI), as a consequence of the hydrogen bubbles generated at these overpotentials, which restrict the access of the electrolyte into the inner porous structure [14]. Furthermore, the electrode ED1 shows the highest values of f_r as a consequence of the lowest Ni loading, thus generating the most porous structure with an increase of 61% and 48% in the real active surface area in comparison with the electrodes ED2 and ED3, respectively. ED1 structure allows better access of the electrolyte to the cathode surface and consequently, easier hydrogen release from the active sites of the porous electrode can take place. In contrast, longer Ni deposition time allowed covering the underlying Cu foam, producing a decrease in the real active surface area. Note that ED3 electrode provides a porous layer with a slight increase of the real active surface area with respect to the ED2 cathode. Ni deposition time of 45 min is sufficient to completely cover the underlying Cu foam and also to generate an external denser Ni porous structure. Nevertheless, the slight increase of the active surface area of ED3 with respect to ED2 does not contribute to any real improvement in the activity under operating conditions.

Intrinsic catalytic activity for HER of the different synthetized electrodes was assessed correcting the exchange current density by the surface roughness factor ($j_o \times f_r^{-1}$), Table 5. According to these results, higher Ni amount provides an improvement in the intrinsic activity although it does not compensate the reduction of the apparent catalytic activity produced by the decreased real active surface area. Therefore, the improvement in the catalytic activity towards HER obtained on the electrode ED1 is mainly due to an enhancement of the real active surface area, without showing apparently any synergetic effect between Ni and Cu.

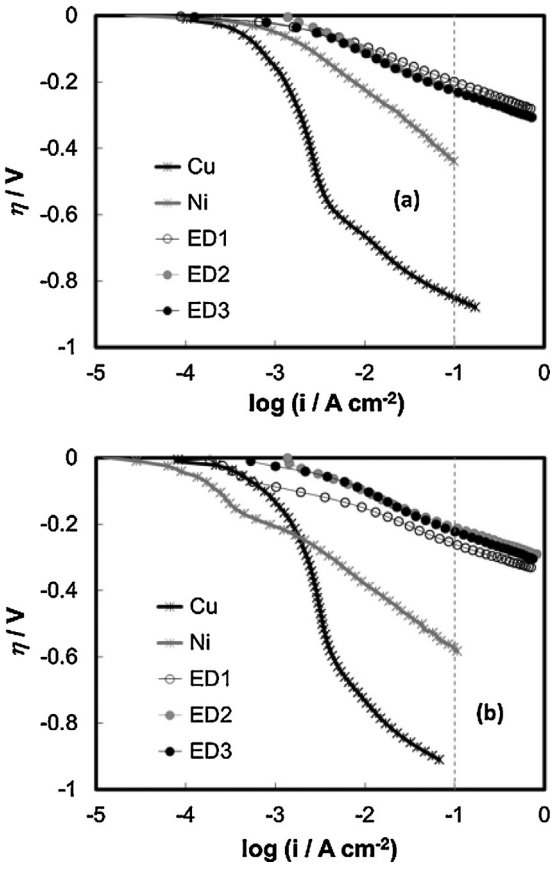

Fig. 7. Linear Tafel polarization curves recorded on Cu, Ni and the different developed cathodes (ED1, ED2 and ED3) in 30 wt.% KOH solution at 80 °C (scan rate 1 mV s^{-1}) after (a) 0.25 V and (b) 0.75 V potentiostatic tests represented in Fig. S2.

3.3. Stability of the synthetized cathodes

3.3.1. First service life test: effect of anodic polarization in the catalytic activity for HER

Polarization curves obtained after the potentiostatic test at 0.25 V for the studied electrodes are shown in Fig. 7(a), and the characteristic electrochemical parameters are summarized in Table 3. For all cathodes, a decrease in η_{100} together with an increase in j_0 is observed after applying 0.25 V. This indicates an improvement of the apparent catalytic activity which can only be consequence of the Cu- and Ni-oxide formation, favored at this applied bias. In addition, ED1 shows the best performance in terms of apparent catalytic activity with the lowest value of $|\eta_{100}|$ (200 mV) and also the highest j_o (1.03 mA cm^{-2}).

EIS were also measured at different cathodic overpotentials following the procedure described in the experimental section. Electrical elements obtained after fitting the experimental results with the EEC shown in Fig. 6 were also included in Table 4. Fig. 8 represents the 3D- diagram of the surface roughness factor (f_r) determined from the C_{dl} values (Table 4) for the investigated cathodes at different overpotentials and after applying the selected anodic potentials.

A decrease in the real surface area was observed after applying 0.25 V in all the developed electrodes. The oxides formed at 0.25 V are occluded inside the macroporous structure hindering the access of the reactive species to the surface. Both the decrease of the active surface area and the increase in the catalytic activity reported in all the studied cathodes leads to the conclusion that the presence of oxide into the porous structure favors the intrinsic catalytic activity of them towards HER (Table 5). Moreover, ED1 shows the best per-

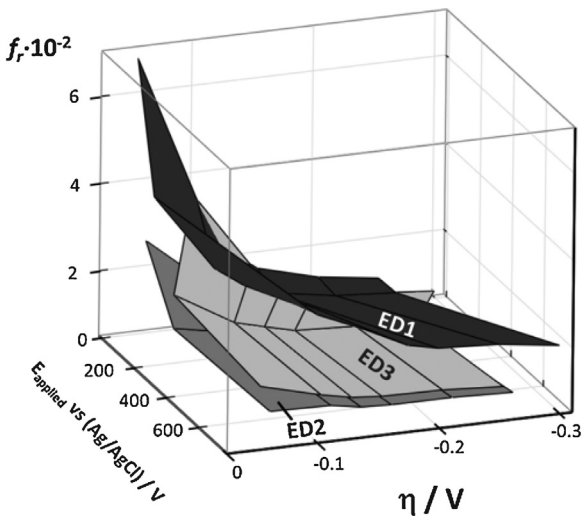

Fig. 8. 3D-representation of the roughness factor (f_r) obtained for the investigated electrocatalytic cathodes in 30 wt.% KOH solution at 80 °C.

formance among all the cathodes for hydrogen production which is mainly due to the presence of CuO/Cu(OH)$_2$ oxides (increase of the catalytic activity of 91% even though active surface area decreases in 33%), Table S2 in SI. Comparing the polarization curves obtained on the Cu smooth electrode (Figs. 4 and 7) and the parameters collected in Table 3, a slight improvement in the catalytic activity is only detected for Cu after the anodic polarization at 0.25 V. Therefore, the significant improvement of the catalytic effect for ED1 electrode towards HER, after applying 0.25 V, can only be attributed to the synergistic interaction between CuO/Cu(OH)$_2$ and β-Ni(OH)$_2$ species. In this case, the synergisms between Cu and Ni metals is clearly observed [23,26–28], which is enhanced by the existence of oxidized species. It is important to highlight that, although Ni and Cu do not alloy in the synthetized cathodes, the oxide products of both metals are in close interfacial contact, thus allowing the modification of the electronic distribution of the system and improving the activity towards the HER. The Ni/Cu ratio in the ED2 cathode seems to be not enough to show the synergistic behavior reported for ED1 cathode.

As a consequence of the oxide formation, the reaction mechanism for hydrogen production can proceed through the reduction of the oxide on the electrode surface, described in the Reactions (14) and (15) [10]:

$$M - OH + H_2O + e^- \rightleftarrows M - OH_2 + OH^- \quad (14)$$

$$M - OH_2 + H_2O + e^- \rightleftarrows M - OH + H_2 + OH^- \quad (15)$$

Or by the direct formation of a M—H bond, Reactions (16) and (17):

$$M - OH_2 + e^- \rightleftarrows M - H + OH^- \quad (16)$$

$$M - H + H_2O \rightleftarrows M - OH + H_2 \quad (17)$$

where M represents Cu and/or Ni metals. As both M-OH and M-OH$_2$ have lower bond strength interaction than M-H [24], the equilibria between H adsorption/desorption can be tuned toward a HER intrinsic activity improvement. Thus, apart from the surface area enlargement, two main effects were suggested to explain the increase in HER activity in the studied systems: (i) the synergetic interaction between CuO/Cu(OH)$_2$ and β-Ni(OH)$_2$ oxides and (ii) the modification of the mechanism reaction for HER by the reduction of the oxide.

On the other hand, an increase of the current density was observed in all the studied coatings during the potentiostatic test at 0.75 V (Fig. S2(b), SI), more pronounced for ED2 and ED3 electrodes. It is well known that Ni hydroxide catalyzes the OER [75–77], being the onset value ca. 0.35 V for the synthetized cathodes (Fig. 3). In contrast, the lowest value of current density observed in the ED1 cathode indicates that higher amount of Cu/Cu-oxides can inhibit and/or retard the water oxidation reaction. Deterioration of the cathodes (in terms of the catalytic activity) with respect to the potentiostatic test at 0.25 V was elucidated by the electrochemical measurements extracted for the polarization curves shown in Fig. 7(b) (increase in the $|\eta_{100}|$ and decrease in the j_o) together with the decrease in the extracted f_r (Fig. 8). A loss of the real active area of nearly 50% in all the cathodes (shown in Table S2, SI) was achieved, which denotes that above OER the damage of the electrodes depends on the potential without relevant influence of the electrode composition. Hence, potentials applied in the cathodes under short-circuited operations in alkaline electrolyzers must be below OER in order to avoid a significant damage of Ni/Cu based cathodes.

3.3.2. *Second service life test: effect of successive short-circuited processes in the activity and stability towards HER*

Final cyclic voltammograms of each series, recorded before applying the cathodic polarization at −1.25 V for 300 s, are represented in Fig. 9 for (a) ED1, (b) ED2 and (c) ED3. As already observed in Section 3.1, the first cycle in all synthetized electrodes is characterized by the presence of the peak 1_A which disappears in the following cycles due to the formation of β-Ni(OH)$_2$ non-reducible specie. Moreover, the peaks 2_A (oxidation of β-Ni(OH)$_2$ to β-NiOOH) and 2_C (reduction of β-NiOOH to β-Ni(OH)$_2$) are well defined in the cycles for the three electrodes, being this behavior typical of the Ni-based cathodes [33,35,37,78]. The relation between the charge corresponding to the peaks 2_A and 2_C in the three studied electrodes is around 1, which indicates that the oxidation/reduction of the system β-Ni(OH)$_2$/β-NiOOH is nearly reversible. Nevertheless, the charge associated with these peaks after the cathodic treatment and successive set of 5 cycles progressively increases.

CVs of ED1 show a high contribution of the Cu peaks (especially II_A and I_C), which remain with the successive cycles. The presence of Cu species into the mesoporous structure does not only increase the charge in the oxidation/reduction of the β-Ni(OH)$_2$/β-NiOOH system, but also enhances the catalytic activity of the HER (more current density at the HER onset).

In order to evaluate the evolution of the *catalytic activity towards HER* of the developed electrodes under short-circuit operations, current density at a potential of −1.25 V (onset of HER) was extracted from the last CV of each set (CVs plotted in Fig. 9). The plot of the extracted cathodic current density ($i_{-1.25V}$) *vs.* the number of cycles was shown in Fig. 10(a). In the first cycles, an increase in the cathodic current for all electrodes was registered because of their activation. Electrodes ED2 and ED3 reverse this trend when the number of cycles increases above 9 and 11 respectively, which can be due to the loss of activity (damaging) during the *2SLT*. On the contrary, ED1 shows a continuous increase in the cathodic current density with the number of cycles, from −48 mA cm^{-2} after the first cycle to −57 mA cm^{-2} after the cycle 50 (increase of 16%). This improvement can be related to the enrichment of Cu/Cu-oxides species into the ED1 porous structure, thus activating cathodic current densities. Therefore, Cu species play a crucial role in the catalytic activity for HER when polarization inversion takes place in the system.

In addition, the *recovering of the activity towards H_2 discharge* of the cathodes after short-circuited conditions can also be evaluated by this *2SLT*. Hence, the final current density value registered at the end of each potentiostatic test at −1.25 V (H_2 discharge between each series of 5 CVs) was plotted as a function of the number of cycles (Fig. 10(b)). According to the CVs presented in Fig. 3, at the cathodic potential of −1.25 V, β-NiOOH and Cu-oxides can

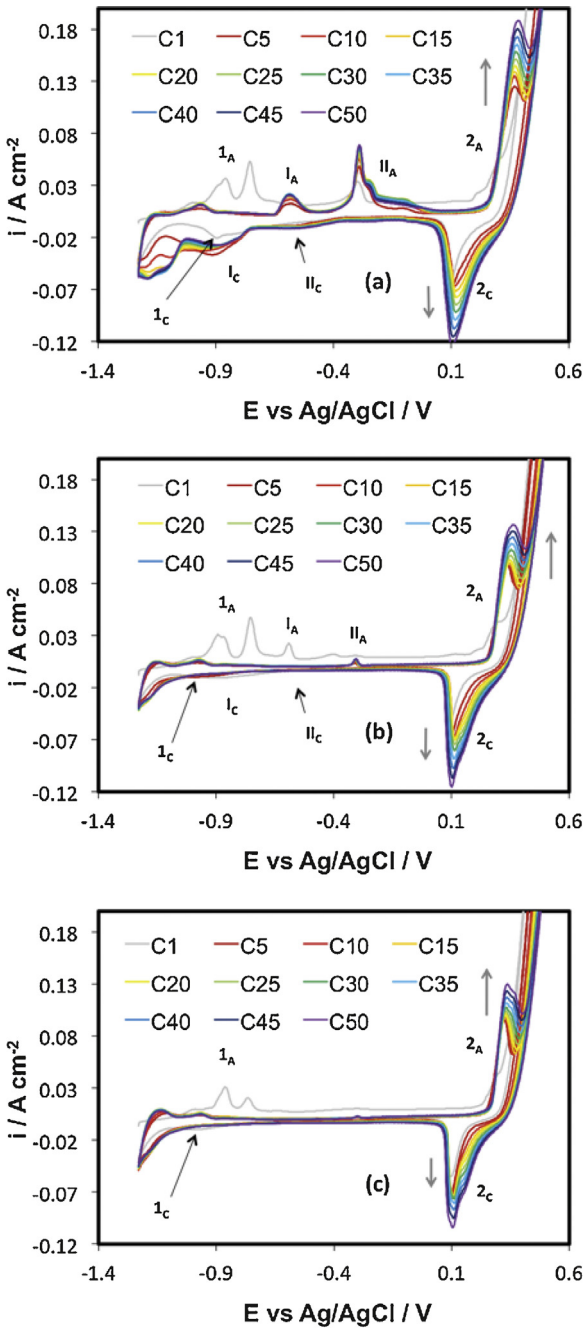

Fig. 9. Evolution of the cyclic voltammograms recorded before each potentiostatic test at −1.25 V onto (a) ED1 (b) ED2 and (c) ED3 at the sweep rate of 50 mV s^{-1} in KOH 30 wt.% at 80 °C in the potential region from hydrogen evolution (−1.25 V) to oxygen evolution (0.5 V).

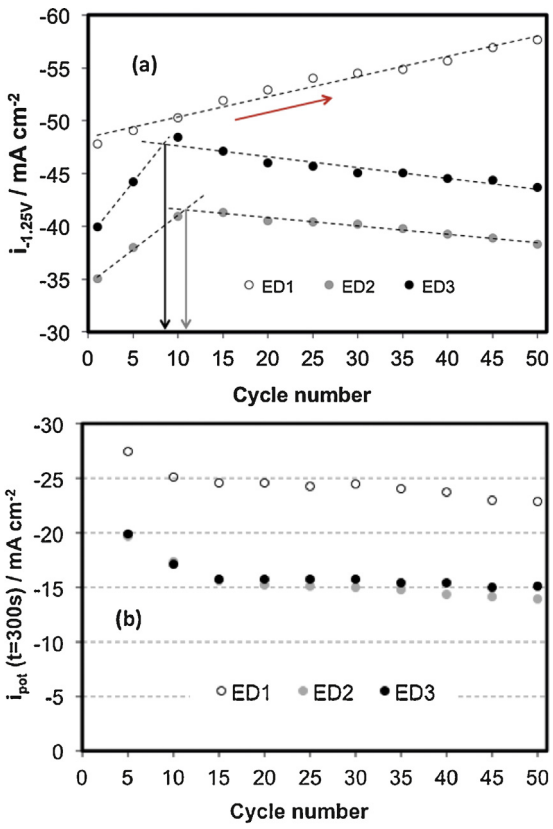

Fig. 10. (a) Average values of the cathodic current densities obtained at the reverse scan of the 5st CV of each series (last cycle previous applying the potentiostatic tests) at the potential of −1.25 V for all three investigated cathodes as a function of the cycle number. (b) Average of the current density obtained at the last minute of the potentiostatic test at −1.25 V (applied during 300 s between series of 5 CVs) for the studied electrocatalysts against cycle number.

be reduced into β-$Ni(OH)_2$ and Cu/Cu_2O species, respectively. In all coatings, a decrease in the cathodic current density with the number of cycles is observed. Jović et al. [35,36] associated this behavior to the continuous damage of the electrodes with the evolution of the long-term tests and the non-recovery of the initial activity conditions. Nevertheless, a constant value of current was observed from cycle 20 indicating a stabilization of the electrode activity. Therefore, an irreversible damage of 13% in ED1, 30% in ED2, and 25% in ED3 was reported, taking into consideration the variation of the cathodic current density extracted for the initial H_2 discharge and after their stabilization in the cycle 20. The authors attributed this effect to the reduction of the oxides (formed on the electrode surface during cycling in the region of oxygen evolution) when the cathodic potential was applied, which becomes in the surface stabilization after certain number of cycles (20 in our case). The highest values of the cathodic current density registered in ED1 confirms its good catalytic activity (catalyzing H_2 discharge), due to the presence of Cu into the Ni-mesostructure and also to the enhancement of the real surface area in comparison with ED2 and ED3 electrodes. On the other hand, the amount of Cu in the ED2 and ED3 cathodes is not sufficient to present that catalytic activity observed in ED1. Therefore, according to the presented results, ED1 shows the best activity towards H_2 discharge after applying successive short-circuited conditions presenting a promising alternative for cathodes in alkaline water electrolysis systems.

It is important to mention that the *2SLT* allows one to evaluate the general apparent activity of the process (principal factor to take into account under operation conditions in industrial electrolyzers), although it does not give information about the contribution of other parameters such as the active surface area. Nevertheless, this *Service Life Test* let us to simulate industrial condition of the electrodes used in the alkaline electrolyzers and how the short-circuited condition affects the apparent activity of the synthetized electrodes.

4. Conclusions

Ni/Cu porous electrodes were synthetized using different Ni electrodeposition times (15 (ED1), 30 (ED2) and 45 (ED3) min) on Cu foams obtained from electrochemical hydrogen bubbles dynamic templates. The electrocatalytic performance of the catalyst electrodes and their stability towards HER was evaluated in

30 wt.% KOH at 80 °C (industrial conditions in alkaline electrolyzers) by electrochemical techniques. Service Life Tests, simulating common and particular operating conditions of alkaline electrolyzers, were successfully designed and implemented, and can be established as basic protocols for a next characterization step of cathodes. From the obtained results, the following conclusions can be drawn:

- The as-prepared cathode with the lowest amount of electrodeposited Ni (33.41% of Cu, ED1) provides the best performance of catalytic activity for HER, mainly due to the enhancement of the real electrochemical surface area. ED2 cathode (with an exposed Cu content of 9.81%) offers the best intrinsic activity, although does not compensate the catalytic improvement of ED1 towards HER reported by the increase in active area.
- Anodic potential of 0.25 V applied on the EDs cathodes produces a considerable decrease of the electrochemical real surface area in all the electrodes due to the filling of the porous structure with oxide species. Nevertheless, a considerable increase of the intrinsic catalytic towards HER (mainly in ED1) was reported. This improvement of the apparent catalytic for HER is essentially due to the formation of $CuO/Cu(OH)_2$ and β-$Ni(OH)_2$ oxides species created during the potentiostatic treatment. The enhancement of the catalytic activity for HER in ED1 after this treatment confirms the synergism between the properties of Cu- and of Ni-oxides.
- Higher anodic potentials (above OER, 0.75 V) produced a significant damage of the cathodes. A half reduction of the real active surface area in all of them, attributed to the formation of nickel hydroxide (OER catalyst) was reported. Therefore, cathodes for alkali-water electrolysis based on Ni must be subjected to potentials below 0.75 V under conditions of inversion polarization.
- Loss of activity towards HER was stabilized after 20 cycles of the designed *Service Life Test* (2SLT) for all the synthetized cathodes. Based on the H_2 discharge after inversion polarization, an irreversible damage of 13%, 30% and 25% was obtained for the electrodes ED1, ED2 and ED3, respectively. In addition, ED1 provides the best apparent activity towards HER during the entire *Service Life Test* (i.e. the highest cathodic current density during the studied cycles). On the other hand, a continuous increase of the current at the HER onset is obtained in ED1 during the successive cycles (simulating conditions of short-circuited situations), thus modifying the monitored trend of ED2 and ED3, where a loss of the activation can be detected after the cycle 11 and 9, respectively.
- ED1 electrode can be considered as a promising cathode in alkaline water electrolyzers, in terms of HER activity and stability under long-term operations. High active surface area together with the interaction between Cu (present into the mesoporous structure) and Ni play an important role in the catalytic activity towards HER, providing also satisfactory results under *Service Life* operation. A Ni/Cu ratio above 90/10 must be reached in order to get synergistic interaction between Ni and Cu.

Acknowledgements

The authors gratefully acknowledge financial support given by the *Generalitat Valenciana* (PROMETEO/2010/023) and Spanish Government (*Ministerio de Ciencia e Innovación*) for the postgraduate grants AP2007-01243 (Carlos Valero-Vidal) and AP2007-03737 (Isaac Herraiz-Cardona).

Appendix A. Supplementary data

Supplementary data associated with this article can be found, in the online version, at http://dx.doi.org/10.1016/j.apcatb.2016.05.030.

References

[1] M.S. Dresselhaus, I.L. Thomas, Alternative energy technologies, Nature 414 (2001) 332–337.
[2] J.A. Turner, A realizable renewable energy future, Science 285 (1999) 687–689.
[3] J.A. Turner, Sustainable hydrogen production, Science 305 (2004) 972–974.
[4] T.N. Veziroglu, F. Barbir, Hydrogen: the wonder fuel, Int. J. Hydrogen Energy 17 (1992) 391–404.
[5] J.O. Bockris, T.N. Veziroglu, A solar-hydrogen economy for U.S.A, Int. J. Hydrogen Energy 8 (1983) 323–340.
[6] W.B. El-Osta, T.N. Veziroglu, Solar-hydrogen energy system for a Libyan coastal county, Int. J. Hydrogen Energy 15 (1990) 33–44.
[7] A.G. García-Conde, F. Rosa, Solar hydrogen production: a Spanish experience, Int. J. Hydrogen Energy 18 (1993) 995–1000.
[8] N. Krstajic, M. Popovic, B. Grgur, M. Vojnovic, D. Sepa, On the kinetics of the hydrogen evolution reaction on nickel in alkaline solution Part I. The mechanism, J. Electroanal. Chem. 512 (2001) 16–26.
[9] M.B.I. Janjua, R.L. Le Roy, Electrocatalyst performance in industrial water electrolysers, Int. J. Hydrogen Energy 10 (1985) 11–19.
[10] A. Lasia, Hydrogen evolution reaction, in: W. Vielstich, A. Lamm, H.A. Gasteiger, H. Yokokawa (Eds.), Handb. Fuel Cells. Fundam. Technol. Appl., John Wiley and Sons, Inc., 2010, pp. 1–25.
[11] Y. Choquette, L. Brossard, A. Lasia, H. Menard, Study of the kinetics of hydrogen evolution reaction on Raney nickel composite-coated electrode by AC impedance technique, J. Electrochem. Soc. 137 (1990) 1723–1730.
[12] Y. Choquette, L. Brossard, A. Lasia, H. Ménard, Investigation of hydrogen evolution on Raney-nickel composite-coated electrodes, Electrochim. Acta 35 (1990) 1251–1256.
[13] C. Hitz, A. Lasia, Experimental study and modeling of impedance of the her on porous Ni electrodes, J. Electroanal. Chem. 500 (2001) 213–222.
[14] V. Ganesh, V. Lakshminarayanan, Preparation of high surface area nickel electrodeposit using a liquid crystal template technique, Electrochim. Acta 49 (2004) 3561–3572.
[15] C.A. Marozzi, A.C. Chialvo, Development of electrode morphologies of interest in electrocatalysis. Part 1: electrodeposited porous nickel electrodes, Electrochim. Acta 45 (2000) 2111–2120.
[16] A.B. Papandrew, T.A. Zawodzinski Jr., Nickel catalysts for hydrogen evolution from CsH_2PO_4, J. Power Sources 245 (2014) 171–174.
[17] B. Pierozynski, T. Mikolajczyk, I.M. Kowalski, Hydrogen evolution at catalytically-modified nickel foam in alkaline solution, J. Power Sources 271 (2014) 231–238.
[18] I. Arul Raj, K.I. Vasu, Transition metal-based cathodes for hydrogen evolution in alkaline solution: electrocatalysis on nickel-based ternary electrolytic codeposits, J. Appl. Electrochem. 22 (1992) 471–477.
[19] J.Y. Huot, M.L. Trudeau, R. Schulz, Low hydrogen overpotential nanocrystalline Ni-Mo cathodes for alkaline water electrolysis, J. Electrochem. Soc. 138 (1991) 1316–1321.
[20] C. González-Buch, I. Herraiz-Cardona, E. Ortega, J. García-Antón, V. Pérez-Herranz, Synthesis and characterization of macroporous Ni, Co and Ni–Co electrocatalytic deposits for hydrogen evolution reaction in alkaline media, Int. J. Hydrogen Energy 38 (2013) 10157–10169.
[21] M. Jafarian, O. Azizi, F. Gobal, M.G. Mahjani, Kinetics and electrocatalytic behavior of nanocrystalline CoNiFe alloy in hydrogen evolution reaction, Int. J. Hydrogen Energy 32 (2007) 1686–1693.
[22] H.J. Miao, D.L. Piron, Composite-coating electrodes for hydrogen evolution reaction, Electrochim. Acta 38 (1993) 1079–1085.
[23] Z. Yin, F. Chen, A facile electrochemical fabrication of hierarchically structured nickel–copper composite electrodes on nickel foam for hydrogen evolution reaction, J. Power Sources 265 (2014) 273–281.
[24] R. Subbaraman, D. Tripkovic, K.-C. Chang, D. Strmcnik, A.P. Paulikas, P. Hirunsit, M. Chan, J. Greeley, V. Stamenkovic, N.M. Markovic, Trends in activity for the water electrolyser reactions on 3d M(Ni, Co, Fe, Mn) hydr(oxy)oxide catalysts, Nat. Mater. 11 (2012) 550–557.
[25] J.O. Bockris, B.E. Conway, E. Yeager, R.E. White, Comprehensive Treatise of Electrochemistry, Plenum Press, New York (USA), 1981.
[26] R. Solmaz, A. Döner, G. Kardas, Electrochemical deposition and characterization of NiCu coatings as cathode materials for hydrogen evolution reaction, Electrochem. Commun. 10 (2008) 1909–1911.
[27] K. Ngamlerdpokin, N. Tantavichet, Electrodeposition of nickel-copper alloys to use as a cathode for hydrogen evolution in an alkaline media, Int. J. Hydrogen Energy 39 (2014) 2505–2515.
[28] R. Solmaz, A. Döner, G. Kardaş, The stability of hydrogen evolution activity and corrosion behavior of NiCu coatings with long-term electrolysis in alkaline solution, Int. J. Hydrogen Energy 34 (2009) 2089–2094.
[29] K. Zeng, D. Zhang, Recent progress in alkaline water electrolysis for hydrogen production and applications, Prog. Energy Combust. Sci. 36 (2010) 307–326.

[30] C.K. Dyer, Improved nickel anodes for industrial water electrolyzers, J. Electrochem. Soc. 132 (1985) 64–67.
[31] A. Manabe, M. Kashiwase, T. Hashimoto, T. Hayashida, A. Kato, K. Hirao, I. Shimomura, I. Nagashima, Basic study of alkaline water electrolysis, Electrochim. Acta 100 (2013) 249–256.
[32] S. Marini, P. Salvi, P. Nelli, R. Pesenti, M. Villa, M. Berrettoni, G. Zangari, Y. Kiros, Advanced alkaline water electrolysis, Electrochim. Acta 82 (2012) 384–391.
[33] N.V. Krstajić, V.D. Jović, L. Gajić-Krstajić, B.M. Jović, a. L. Antozzi, G.N. Martelli, Electrodeposition of Ni-Mo alloy coatings and their characterization as cathodes for hydrogen evolution in sodium hydroxide solution, Int. J. Hydrogen Energy 33 (2008) 3676–3687.
[34] C. Iwakura, M. Tanaka, S. Nakamatsu, H. Inoue, M. Matsuoka, N. Fuujkawa, Electrochemical properties of Ni/(Ni + RuO_2) active cathodes for hydrogen evolution in clor-alkaline electrolysis, Electrochim. Acta 40 (1995) 977–982.
[35] V.D. Jović, U. Lačnjevac, B.M. Jović, N.V. Krstajić, Service life test of non-noble metal composite cathodes for hydrogen evolution in sodium hydroxide solution, Electrochim. Acta 63 (2012) 124–130.
[36] B.M. Jović, U.Č. Lačnjevac, N.V. Krstajić, V.D. Jović, Service life test of the NiSn coatings as cathodes for hydrogen evolution in industrial chlor-alkali electrolysis, Int. J. Hydrogen Energy 39 (2014) 8947–8958.
[37] A.L. Antozzi, C. Bargioni, L. Iacopetti, M. Musiani, L. Vázquez-Gómez, EIS study of the service life of activated cathodes for the hydrogen evolution reaction in the chlor-alkali membrane cell process, Electrochim. Acta 53 (2008) 7410–7416.
[38] R. Solmaz, A. Döner, I. Şahin, A.O. Yüce, G. Kardaş, B. Yazici, M. Erbil, The stability of NiCoZn electrocatalyst for hydrogen evolution activity in alkaline solution during long-term electrolysis, Int. J. Hydrogen Energy 34 (2009) 7910–7918.
[39] I. Herraiz-Cardona, E. Ortega, V. Pérez- Herranz, Impedance study of hydrogen evolution on Ni/Zn and Ni–Co/Zn stainless steel based electrodeposits, Electrochim. Acta 56 (2011) 1308–1315.
[40] I. Herraiz-Cardona, E. Ortega, L. Vázquez-Gómez, V. Pérez-Herranz, Electrochemical characterization of a NiCo/Zn cathode for hydrogen generation, Int. J. Hydrogen Energy 36 (2011) 11578–11587.
[41] I. Herraiz-Cardona, E. Ortega, J.G. Antón, V. Pérez-Herranz, Assessment of the roughness factor effect and the intrinsic catalytic activity for hydrogen evolution reaction on Ni-based electrodeposits, Int. J. Hydrogen Energy 36 (2011) 9428–9438.
[42] I. Herraiz-Cardona, E. Ortega, L. Vázquez-Gómez, V. Pérez-Herranz, Double-template fabrication of three-dimensional porous nickel electrodes for hydrogen evolution reaction, Int. J. Hydrogen Energy 37 (2012) 2147–2156.
[43] J. García-Antón, A. Igual Muñoz, J.L. Guiñón, V. Pérez-Herranz, P200002526 (2000).
[44] L.E.A. Berlouis, D.A. Mamman, I.G. Azpuru, The electrochemical behaviour of copper in alkaline solutions containing fluoride, studied by in situ ellipsometry, Surf. Sci. 408 (1998) 173–181.
[45] M. Pourbaix, Atlas of Electrochemical Equilibria in Aqueous Solutions, 2nd ed., National Association of Corrosion Engineers, Pergamon Press, Oxford, London (United Kingdom), 1974.
[46] H.H. Strehblow, B. Titze, The investigation of the passive behaviour of copper in weakly acid and alkaline solutions and the examination of the passive film by esca and ISS, Electrochim. Acta 25 (1980) 839–850.
[47] H.D. Speckmann, S. Haupt, H. Strehblow, A quantitative surface analytical study of electrochemically-formed copper oxides by XPS and X-ray-Induced auger Sp & troscopy, Surf. Interface Anal. 11 (1988) 148–155.
[48] J. Kunze, V. Maurice, L.H. Klein, H.-H. Strehblow, P. Marcus, In situ STM study of the duplex passive films formed on Cu (111) and Cu(001) in 0.1 M NaOH, Corros. Sci. 46 (2004) 245–264.
[49] L.D. Burke, M.J.G. Ahern, T.G. Ryan, An investigation of the anodic behavior of copper and its anodically produced oxides in aqueous solutions of high pH, J. Electrochem. Soc. 137 (1990) 553–561.
[50] A. Seyeux, V. Maurice, L.H. Klein, P. Marcus, In situ scanning tunnelling microscopic study of the initial stages of growth and of the structure of the passive film on Ni(111) in 1 mM NaOH(aq), J. Solid State Electrochem. 9 (2005) 337–346.
[51] A. Seghiouer, J. Chevalet, A. Barhoun, F. Lantelme, Electrochemical oxidation of nickel in alkaline solutions: a voltammetric study and modelling, J. Electroanal. Chem. 442 (1998) 113–123.
[52] K. Juodkazis, J. Juodkazytė, R. Vilkauskaitė, V. Jasulaitienė, Nickel surface anodic oxidation and electrocatalysis of oxygen evolution, J. Solid State Electrochem. 12 (2008) 1469–1479.
[53] D.S. Hall, C. Bock, B.R. MacDougall, The electrochemistry of metallic nickel: oxides, hydroxides, hydrides and alkaline hydrogen evolution, J. Electrochem. Soc. 160 (2013) F235–F243.
[54] D. Pletcher, R. Greff, R. Peat, L.M. Peter, J. Robinson, Instrumental Methods in Electrochemistry, Woodhead Publishing Limited, 2001.
[55] I. Herraiz-Cardona, Doctoral Thesis: Desarrollo de nuevos materiales de electrodo para la obtención de Hidrógeno a partir de la electrólisis alcalina del agua (2012).
[56] Southampton Electrochemistry Group, Instrumental Methods in Electrochemistry, Ellis Horwood Ltd, New York (USA), 1985.
[57] J.O. Bockris, A.K.N. Reddy, M. Gamboa- Aldeco, Modern Electrochemistry. Fundamentals of Electrodics, vol. 2A, Se, Kluwer Academic Publishers, New York (USA), 2000.
[58] A. Lasia, A. Rami, Kinetics of hydrogen evolution on nickel electrodes, J. Electroanal. Chem. Interfacial Electrochem. 294 (1990) 123–141.
[59] F. Rosalbino, G. Scavino, M. Actis Grande, Electrocatalytic activity of Ni–Fe–M (M = Cr, Mn Cu) sintered electrodes for hydrogen evolution reaction in alkaline solution, J. Electroanal. Chem. 694 (2013) 114–121.
[60] E. Navarro-Flores, Z. Chong, S. Omanovic, Characterization of Ni, NiMo NiW and NiFe electroactive coatings as electrocatalysts for hydrogen evolution in an acidic medium, J. Mol. Catal. A: Chem. 226 (2005) 179–197.
[61] L. Birry, A. Lasia, Studies of the hydrogen evolution reaction on Raney nickel-molybdenum electrodes, J. Appl. Electrochem. 34 (2004) 735–749.
[62] I. Herraiz-Cardona, C. González-Buch, C. Valero-Vidal, E. Ortega, V. Pérez-Herranz, Co-modification of Ni-based type Raney electrodeposits for hydrogen evolution reaction in alkaline media, J. Power Sources 240 (2013) 698–704.
[63] R.D. Armstrong, M. Henderson, Impedance plane display of a reaction with an adsorbed intermediate, Electroanal. Chem. Interfacial Electrochem. 39 (1972) 81–90.
[64] D.A. Harrington, B.E. Conway, ac Impedance of faradaic reactions involving electrosorbed intermediates—I. Kinetic theory, Electrochim. Acta 32 (1987) 1703–1712.
[65] N.A. Assunçào, M.J. de Giz, G. Tremilioso- Filho, E.R. Gonzalez, A study of the hydrogen evolution reaction on a Ni/NiFeS electrodeposited coating, J. Electrochem. Soc. 144 (1997) 2794–2800.
[66] L. Bai, D.A. Harrington, B.E. Conway, Behavior of overpotential-deposited species in faradaic reactions—II. ac Impedance measurements on H_2 evolution kinetics at activated and unactivated Pt cathodes, Electrochim. Acta 32 (1987) 1713–1731.
[67] A. Lasia, Electrochemical impedance spectroscopy and its applications, in: B.E. Conway, J. Brockris, R.E. White (Eds.), Mod. Asp. Electrochem., Springer US, New York (USA), 1999, pp. 143–248.
[68] C. Valero Vidal, A. Igual Muñoz, Electrochemical characterisation of biomedical alloys for surgical implants in simulated body fluids, Corros. Sci. 50 (2008) 1954–1961.
[69] C. Valero Vidal, A. Igual Muñoz, Electrochemical aspects in biomedical alloy characterization: electrochemical impedance spectroscopy, in: A.N. Laskovski (Ed.), Biomed. Eng. Trends Mater. Sci., InTech, 2011, 2016, pp. 283–306.
[70] G.J. Brug, A.L.G. Van den Eeden, M. Sluyters- Rehbach, J.H. Sluyters, The analysis of electrode impedances complicated by the presence of a constant phase element, J. Electroanal. Chem. 176 (1984) 275–295.
[71] C. Valero Vidal, A. Igual Muñoz, Study of the adsorption process of bovine serum albumin on passivated surfaces of CoCrMo biomedical alloy, Electrochim. Acta 55 (2010) 8445–8452.
[72] L. Chen, A. Lasia, Study of the kinetics of hydrogen evolution reaction on nickel–zinc alloy electrodes, J. Electrochem. Soc. 138 (1991) 3321–3328.
[73] A. Rami, A. Lasia, Kinetics of hydrogen evolution on Ni–Al alloy electrodes, J. Appl. Electrochem. 22 (1992) 376–382.
[74] L. Chen, A. Lasia, Study of the kinetics of hydrogen evolution reaction on nickel–zinc powder electrodes, J. Electrochem. Soc. 139 (1992) 3214–3219.
[75] D.A. Corrigan, R.M. Bendert, Effect of coprecipitated metal ions on the electrochemistry of nickel hydroxide thin films: cyclic voltammetry in 1 M KOH, J. Electrochem. Soc. 136 (1989) 723–728.
[76] J. Kubisztal, A. Budniok, Study of the oxygen evolution reaction on nickel-based composite coatings in alkaline media, Int. J. Hydrogen Energy 33 (2008) 4488–4494.
[77] M.F. Kibria, M.S. Mridha, Electrochemical studies of the nickel electrode for the oxygen evolution reaction, Int. J. Hydrogen Energy 21 (1996) 179–182.
[78] A. Pătru, P. Antitomaso, R. Sellin, N. Jerez, P.L. Taberna, F. Favier, Size and strain dependent activity of Ni nano and micro particles for hydrogen evolution reaction, Int. J. Hydrogen Energy 38 (2013) 11695–11708.